Journal of Nuclear Materials 446 (2014) 56–62

Contents lists available at ScienceDirect

Journal of Nuclear Materials

journal homepage: www.elsevier.com/locate/jnucmat

Modeling hydrogen isotope behavior in fusion plasma-facing components

Alice Hu *, Ahmed Hassanein

Center for Materials Under Extreme Environment, School of Nuclear Engineering, Purdue University, West Lafayette, IN 47906, USA

ARTICLE INFO

Article history:
Received 15 August 2013
Accepted 25 November 2013
Available online 28 November 2013

ABSTRACT

In this work, we focus on understanding hydrogen isotope retention in plasma-facing materials in fusion devices. Three common simulation methods are usually used to study this problem that includes Monte Carlo, molecular dynamics, and numerical/analytical methods. A system of partial differential equations describing deuterium behavior in tungsten under various conditions is solved numerically to explain recent data compared to other methods. The developed model of hydrogen retention in metals includes classic, intercrystalline and trapped-induced Gorsky effects. The bombardment and depth profile of 200 eV deuterium in single crystal tungsten are simulated and compared with recent work. The total deuterium retention at various temperatures and fluences are also calculated and compared with available data. The results are in reasonable agreement with data and therefore, this model can be used to estimate deuterium inventory and recovery in future fusion devices.

1. Introduction

Magnetic fusion energy is a promising next generation source of electricity. The choice of plasma-facing components (PFCs) is a key engineering challenge in fusion reactor design since the interactions between plasma and PFCs are directly related to fuel lost, safety, and wall recovery issues. Carbon, beryllium, and tungsten have been chosen to be the primary materials in the International Thermonuclear Experimental Reactor (ITER). Tungsten has become an essential material in fusion reactor design because of its low erosion yield and high melting point. Therefore, hydrogen isotopes retention and migration in tungsten has transpired into an important safety issue. Consequently, transport and trapping properties of hydrogen isotopes in tungsten is crucial and need further understanding.

Fig. 1 shows a typical hydrogen isotope spatial profile in metal. It is observed in metals such as tungsten [1] which is the focus of this research, as well as stainless steel 304 and 316 [2], molybdenum [3] and Inconel (nickel–chromium based alloy) [2]. Hydrogen isotopes spatial distribution in metal can be generally divided into three regions: near-surface region (I), sub-surface region (II), and bulk (III). The near-surface region has higher concentration due to the incoming hydrogen being implanted and trapped in a few nanometers thickness layer. The sub-surface region shows the classic peak profile of atomic diffusion in metal lattice. In the bulk region, the concentration becomes more flat and slowly decaying and does not change much as hydrogen diffusion extends into the bulk.

In order to explain such spatial profile and the "uphill diffusion" in region II, the classic Gorsky effect is utilized. The Gorsky effect is a diffusion relaxation process first predicted by W.S. Gorsky in 1935 [4], and is observed 30 years later in experiments by Schaumann and Alefeld [5] and Cantelli [6]. The Gorsky effect occurs when two conditions are fulfilled: First the point defects need to produce host lattice distortion and change the metal volume, which is true for almost every defect. Secondly, the defect mobility needs to be high enough in order to be observed [6]. Therefore, Gorsky effect is mostly seen in hydrogen-metal systems. For instance, if we bend a beamlike sample, the result would be a stress gradient in the sample and cause interstitial atoms to migrate from the compressive side to the stretching side as schematically shown in Fig. 2.

In 2000, H.R. Sinning first proposed the "intercrystalline Gorsky effect" (IGE) [7,8]. Sinning described IGE as a new relaxation mechanism for hydrogen diffusion in local stress field due to mismatch strain in polycrystalline. Despite the external bending in classical case, the stress gradient is now generated from internal misfits within grains and at grain boundaries. Sinning's research focuses on measuring dissipation factor and utilizes IGE to explain the broad damping spectrum of hydrogen diffusion in intermetallic compounds. However there is no detail mathematical description of how hydrogen reacts in metal stress field.

As the hydrogen concentration peak shown in region II in Fig. 1, a possible explanation could be that there is a stress field between region I and region II. This stress field ought to be generated from the host lattice distortion by implantation trapped hydrogen in near-surface. Thus, we proposed this stress field as trapped-induced Gorsky effect (TGE). TGE could result in an uphill diffusion

* Corresponding author. Tel.: +1 7654099162.
E-mail address: hu77@purdue.edu (A. Hu).

0022-3115/$ - see front matter © 2013 Elsevier B.V. All rights reserved.
http://dx.doi.org/10.1016/j.jnucmat.2013.11.033

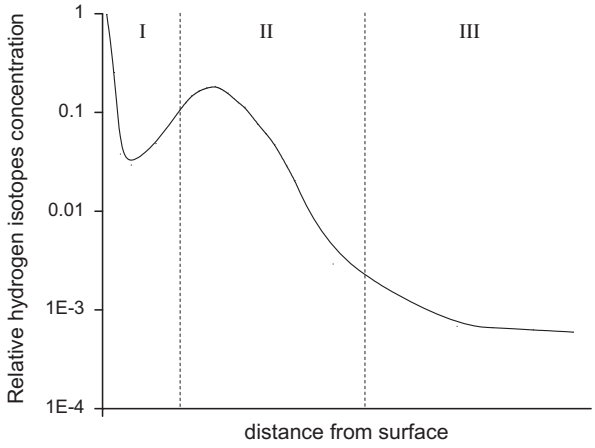

Fig. 1. Hydrogen isotopes depth profile in metal [2].

that is similar to Gorsky effect. The difference is that Gorsky effect depends on external bending stresses while TGE depends on internal lattice distortion. With lattice distortion it would increase the stress and decrease trap sites between region I and region II as illustrated in Fig. 3.

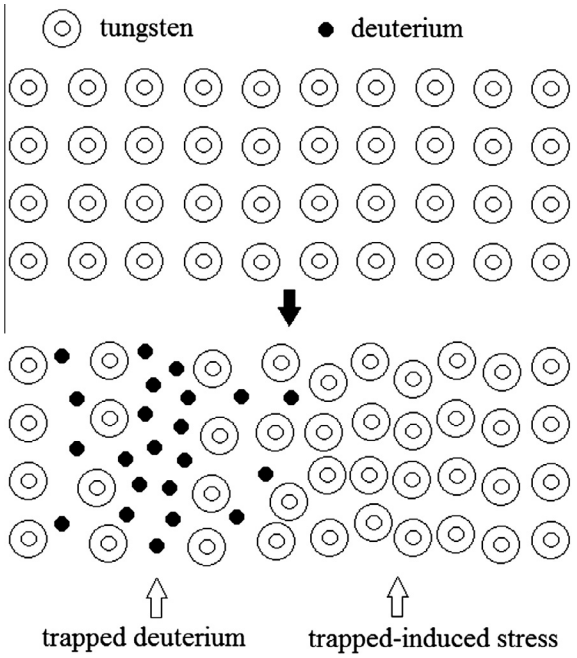

Fig. 3. Possible mechanism of trapped-induced stress.

2. Model and methods

2.1. Major equations, ICs and BCs

Most of the traditional diffusion equations solved in this work are the general Fick diffusion equations and boundary conditions developed for the diffuse code described elsewhere [9] which is the first continuum code for hydrogen transport in wall established by M.I. Baskes. The diffuse code utilizes the diffusion equations for solving ion distribution in materials, with numerous conditions and examples such as those given by Wilson et al. [10]. However the pressure gradient is not considered in the common Fick's first law $J = -D\frac{\partial C}{\partial x}$ and second laws $\frac{dC}{dt} = \frac{\partial}{\partial x}\left(D\frac{\partial C}{\partial x}\right)$ which describe diffusion driven only by concentration gradient. Therefore the diffusion equations need to be modified. We consider the diffusion driven by gradient of chemical potential [11,12]:

$$\mu = \mu^0 + R(\theta - \theta^Z)ln\varphi + p\overline{V}_H$$

where μ^0 is a fixed datum (a standard position or level that measurements are taken from), R is the universal gas constant, θ is temperature, θ^Z is temperature at zero Kelvin, φ is normalized concentration defined by $\varphi = c$ (concentration)/s (solubility), p is the equivalent pressure stress defined as $p = -\text{trace}(\sigma)/3$ and $\overline{V}_H$ is the partial molar volume (the change in volume per mole of hydrogen added to the solid solution). Therefore, the extended flux now includes diffusion driven by temperature and pressure gradients, and is written as [11,12]:

$$J = -sD\left[\frac{\partial\varphi}{\partial x} + \varphi ln\varphi\frac{\partial}{\partial x}(\ln(\theta - \theta^Z)) + \varphi\frac{\overline{V}_H}{R(\theta - \theta^Z)}\frac{\partial p}{\partial x}\right] \quad (1)$$

In our work the equations

$$J = -D\left[\frac{\partial c}{\partial x} + c\frac{\overline{V}_H}{R(\theta - \theta^Z)}\frac{\partial p}{\partial x}\right] \quad (2)$$

$$\text{and } \frac{dC}{dt} = D\frac{\partial^2 C}{\partial x^2} + \frac{Dc\overline{V}_H}{R(\theta - \theta^Z)}\frac{\partial^2 p}{\partial x^2} \quad (3)$$

are used for diffusion induced by concentration and pressure gradients. The general form of p should be calculated from three by three matrix dimension, but since we are doing one-dimensional modeling, and every parameter reduce to degree one in this case, p can simply equals to the pressure value.

The major equations used in the current research for hydrogen isotope behavior in metals can then be written in following:

$$\frac{dC}{dt} = G + D\frac{\partial^2 C}{\partial x^2} + \frac{DC_T\overline{V}_H}{RT}\frac{\partial^2 p}{\partial x^2} - \sum_i \frac{dC_{Ti}}{dt} \quad (4)$$

$$\frac{dC_{Ti}}{dt} = \frac{D}{\lambda^2}C\frac{C^0_{\text{Trapi}} - C_{Ti}}{W} - C_{Ti}\frac{D_0}{\lambda^2}\exp\left(\frac{-E_{Ti}}{kT}\right) \quad (5)$$

where C is the mobile deuterium atomic concentration; C_T is the total deuterium concentration at that position; C_{Ti} is the ith trapped deuterium atomic concentration; G is the implanted deuterium flux; D is the diffusion coefficient; V_H is the partial molar volume; R is the universal gas constant and p is the equivalent pressure

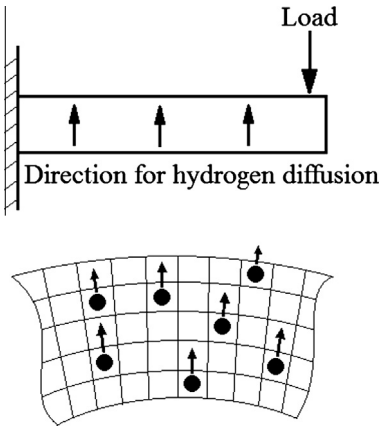

Fig. 2. Migration of interstitial atoms upon sample bending, according to the Gorsky relaxation model [5].

stress; λ is the jump distance; C^0_{Trapi} is the maximum trapping density; W is the tungsten atomic density; D_0 is the diffusion pre-exponential factor; E_{Ti} is the ith detrapping energy; k is the Boltzmann constant, and T is the temperature. This system of differential equations is solved by SUNDIALS [13], where Eq. (4) represent the change for mobile deuterium and Eq. (5) stands for the change in trapped deuterium.

For the right hand side of Eq. (4), G is the implanted deuterium. The second term $D\frac{\partial^2 C}{\partial x^2}$ is the diffusion due to concentration gradient. The third term $\frac{Dc\overline{V}_H}{R(\theta-\theta^2)}\frac{\partial^2 p}{\partial x^2}$ is the diffusion due to stress gradient induced from TGE. The last term $\sum_i \frac{dC_{Ti}}{dt}$ is the amount of mobile deuterium that is changed to trapped concentration. The first term in Eq. (5) $\frac{D}{\lambda^2}C\frac{C^0_{Ti}-C_{Ti}}{W}$ can be viewed as three parts $\frac{D}{\lambda^2}$, C, and $\frac{C^0_{Ti}-C_{Ti}}{W}$. The first part $\frac{D}{\lambda^2}$ is the jump frequency, second part C is the mobile deuterium concentration, and third part $\frac{C^0_{Ti}-C_{Ti}}{W}$ is the fraction of empty traps in tungsten, which means the probability of one mobile deuterium may jump into a trap site nearby. The second term in Eq. (5) is $C_{Ti}\frac{D_0}{\lambda^2}\exp\left(\frac{-E_{Ti}}{kT}\right)$, and it can be viewed as C_{Ti} times $\frac{D_0}{\lambda^2}\exp\left(\frac{-E_{Ti}}{kT}\right)$, which is the trapped deuterium concentration times jump frequency which means probability of a trapped deuterium becomes mobile again.

All trapped and mobile deuterium concentrations in the material are assumed to be zero at the initial conditions. Due to the fact this is a one-dimension simulation, so there are two boundary conditions. The first boundary condition is at the surface ($x = 0$) where ions are coming in, the other boundary condition is the rear side of the material. The total calculation length is estimated by $r = \sqrt{6Dt}$, since r is less than 200 μm in most cases, we used 200 μm as the total distance for the backside length. At $x = 0$, surface recombination flux and moving boundary due to possible erosion or redeposition need to be considered. Deuterium atoms can be recombined with each other and leave the surface in gas form. The equation for such recombination is given by:

$$J_{D_2} = -D\frac{\partial C}{\partial x}\bigg|_{x=0} = K_r C(0)^2 \tag{6}$$

where K_r is recombination coefficient, and when the ion energy is less than the sputtering yield threshold, there is no sputtering as the surface would not erode, otherwise the surface would erode with the rate $= \frac{\text{flux}*\text{sputtering yield}}{\text{tungsten atomic density}}$. The sputtering yield values are obtained from reference [14]. The second boundary condition is at the back surface ($x = 200$ μm), either $C = 0$ *or* $\frac{\partial C}{\partial x} = 0$ can be utilized because most deuterium did not yet diffuse to this depth within time t, and both condition give the same answers.

2.2. Coefficients

The deuterium implantation profile is in normal distribution form as given in Eq. (7) for simplification. The peak and standard deviation are given from the longitudinal range and straggling in Monte Carlo calculation using ITMC [15].

$$G = \text{flux} * \frac{1}{\sigma\sqrt{2\pi}}\exp\frac{-(x-\mu)^2}{2\sigma^2} \tag{7}$$

This assumption is proper because it resembles experimental data and similar assumption is common among other simulations [9,16,17], and sometimes it is even further simplified to a homogeneous distribution on surface [18]. More coefficient values are listed in Table 1.

The diffusion coefficient of $D = 4.1 \times 10^{-7}\exp(-0.39/\text{kT})\ \text{m}^2\ \text{s}^{-1}$ based on work by Frauenfelder [19] has been used in other simulation work [17,18,20]. However, application of this value is inconsistent with our results in the temperature range of 300–800 K. In the results given by Alimov and Roth [1], it can be observed that deuterium gradually diffuse into bulk as temperature goes higher. However, if we perform the simulation using $D = 4.1 \times 10^{-7}\exp(-0.39/\text{kT})$ and only the source and diffusion term as in Eq. (8), the phenomena of gradual diffusion cannot be seen.

$$\frac{dC}{dt} = G + D\frac{\partial^2 C}{\partial x^2} \tag{8}$$

Fig. 4 shows the diffusion result using $D = 4.1 \times 10^{-7}\exp\left(-\frac{0.39}{kT}\right)$ for Eq. (8). The diffusion process is very fast that the concentration

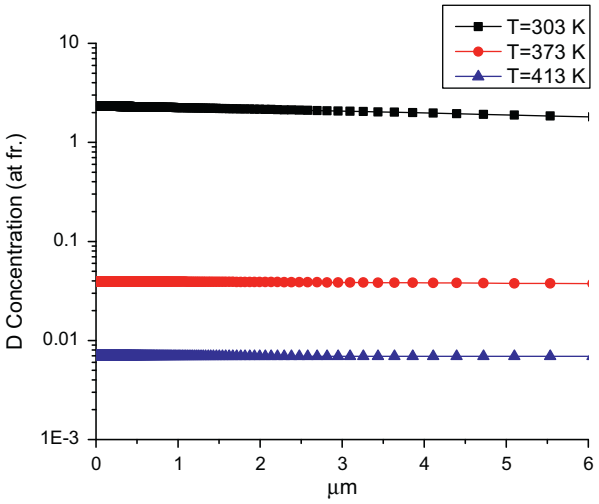

Fig. 4. Deuterium distribution at higher diffusion coefficient.

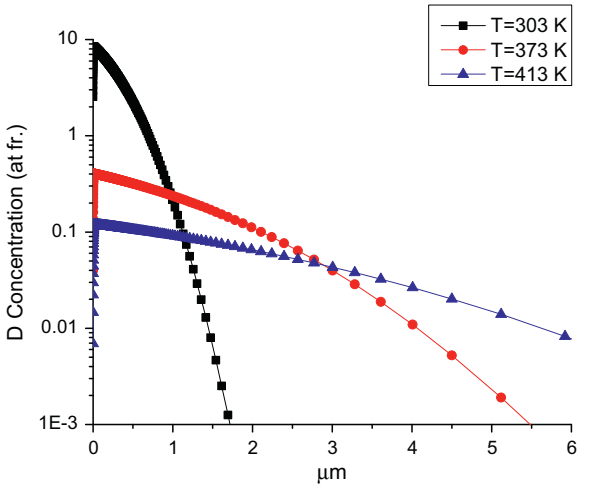

Fig. 5. Deuterium distribution at lower diffusion coefficient.

Table 1
Coefficient values.

	Meaning	Value
D	Diffusivity	$D_0 \times \exp(-E_d/\text{kT})$
D_0	Pre-exponential diffusion coefficient	$1.5 \times 10^{-10}\ \text{m}^2\ \text{s}^{-1}$
E_d	Migration energy	0.39 eV
K_r	Surface recombination coefficient	$K_{r0} \times \exp(-E_r/\text{kT})$
K_{r0}	Pre-exponential recombination coefficient	$3.2 \times 10^{-15}\ \text{m}^4\ \text{s}^{-1}$
E_r	Surface recombination energy	1.16 eV
W	Tungsten atomic density	$6.3057 \times 10^{28}\ \text{m}^{-3}$
D_m	Maximum diffusion coefficient	$10 \times D$
λ	Jump distance	3×10^{-10} m
$\overline{V}_H$	Partial molar volume	$1.68 \times 10^{-6}\ \text{m}^3/\text{mol}$

becomes almost flat near the surface region. If further including trap sites, the deuterium distribution would be very similar to the trap distribution because the mobile deuterium concentration is same everywhere. And this is a possible reason why there is no obvious temperature difference in other simulation work. Since the diffusion coefficient can be composed by segments in different temperature region, the value $D = 1.5 \times 10^{-10}$ exp $(-0.39/\mathrm{kT})$ $\mathrm{m^2\ s^{-1}}$ is selected which is between the modeling values by Franzen et al. [21] (1.5×10^{-10} exp $(-0.25/\mathrm{kT})$ $\mathrm{m^2\ s^{-1}}$) and GarciaRosales et al. [22] (3.5×10^{-11} exp $(-0.39/\mathrm{kT})$ $\mathrm{m^2\ s^{-1}}$). Fig. 5 shows the diffusion result with $D = 1.5 \times 10^{-10}$ exp $(-0.39/\mathrm{kT})$ for Eq. (8). With the lower diffusion coefficient, the gradually diffusion processes can be simulated.

For radiation-enhanced diffusion coefficient, we use the forms as in reference [20]. Radiation-enhanced diffusion coefficient is used at the surface with the form:

$$D(x,t) = D_m\left(1 - \left(1 - \frac{D}{D_m}\right)\exp\left(-\frac{(1-r)I_0\psi(x)\eta t}{\mu_m}\right)\right) \tag{9}$$

From previous research [20], D_m can be five times larger than bulk diffusion coefficient. If larger D_m is implemented, deuterium near surface can be more mobile and thus reduces the accumulated amount at the surface. We assumed D_m is ten times larger than bulk diffusion coefficient for better fitting of the experimental data. However this value needs further studies and its relationship with surface recombination coefficient is not yet clear.

The increase in trap density can be written as [16,20]:

$$\frac{dC_{\mathrm{Trap}}}{dt} = (1-r)\cdot \mathrm{flux}\cdot\psi(x)\cdot\eta\cdot\left(1 - \frac{C_{\mathrm{Trap}}}{C^0_{\mathrm{Trap}}}\right) \tag{10}$$

where C_{Trap} is the trap density; r is the reflection coefficient; $\psi(x)$ is the depth distribution of ion-induced defects; η is the defect creation rate and C^0_{Trap} is the maximum defect concentration. After integration with time t, trap density is obtained as following:

$$C_{\mathrm{Trap}}(x,t) = C^0_{\mathrm{Trap}}\left(1 - exp\left(-(1-r)\cdot\mathrm{flux}\cdot\psi(x)\cdot\eta\cdot\frac{t}{C^0_{\mathrm{Trap}}}\right)\right) \tag{11}$$

For most of the parameters we use the values suggested in reference [20] as in Table 2. Some values are slightly modified for better fitting to the experiment data. Two different kinds of traps are considered here. The traps with 0.85 eV detrapping energy represent dislocation sites and grainboundaries; the traps with 1.45 eV detrapping energy correspond to deuteriun cluster and vacancy trapping. Both trap energies can be divided to intrinsic and ion-induced parts. For the choice of ion-induced defect distribution $\psi(x)$, there are two possible settings [17,20]. The major difference in these two settings is that the peak position of 0.85 eV ion-induced trap distribution is shifted. Considering the trap sites should be reduced in stressed region by TGE, we use similar setting as reference [17].

From the research in hydrogen cracking in metals, the pressure value around crack tip may range from hundreds MPa to even thousand MPa [23,24]. Although the exact pressure induced by stress field from TGE at surface is unknown, we can safely assume it is smaller than the pressure around crack tip. Thus we used a normal distribution with peak value of around 10 MPa for simplification to evaluate the effect of pressure on the diffusion processes.

Surface recombination coefficient is given as 3.2×10^{-15} exp $\left(-1.16\frac{eV}{kT}\right)$ $\mathrm{m^4/s}$ in the work of Anderl et al. [25], which depends on Frauenfelder diffusion coefficient. They measure surface recombination over the temperature range of 690–825 K, if we extrapolate that to 300–500 K region, the value is too small compared to the modeling result from GarciaRosales et al. [22] and Franzen et al. [26]. In the review by Causey [27], surface recombination coefficient values and trend may vary significantly depending on various conditions. Therefore both the pre-exponential factor and activation energy need further investigations.

In calculating the diffusion induced by stress field, one needs to consider partial molar volume of hydrogen in tungsten. Partial molar volume means the volume change when adding one mole of hydrogen into tungsten. We did not find the value for tungsten so we used the partial molar volume of hydrogen in titanium [23] instead.

Table 2
Trapping profile parameters.

E_T	Detrapping energy	0.85, 1.45 (eV)
C^0_{Trap}	0.85 eV Maximum intrinsic traps	3×10^{-5} at fr.
	1.45 eV Maximum intrinsic traps	1×10^{-5} at fr.
	0.85 eV Maximum ion-induced traps	0.005 at fr.
	1.45 eV Maximum ion-induced traps	0.01 at fr
η	0.85 eV Ion-induced defect production rate	2×10^{-3}
	1.45 eV Ion-induced defect production rate	1×10^{-3}

3. Results

3.1. Deuterium depth profile

In this section we simulate and study single crystal tungsten (SCW) exposed to 200 eV deuterium plasma with high flux ($\approx 10^{21}$ D $\mathrm{m^{-2}\ s^{-1}}$) and fluence which is about 2×10^{24} D $\mathrm{m^{-2}}$ at various temperatures (303 K, 373 K, 413 K, 463 K, and 533 K). All results with and without the TGE term $\frac{DC_T\bar{V}_H}{RT}\frac{\partial^2 p}{\partial x^2}$ are compared with the recent experimental data from Alimov and Roth [1].

Fig. 6(a–e) shows that the depth profile extends more into the bulk with increasing temperature. However, in the mean time more deuterium can acquire enough energy to detrap from a trapping site such that the trapped amount could decrease. It should also be noticed that the trapped deuterium around few μm from the surface detrap faster than the surface trapped deuterium because they have lower detrapping energy (0.85 eV) compared to surface traps (1.45 eV). At temperature equals 303 K, the predicted surface recombination value is too low, and this could be the reason that the simulation result predicts much higher concentration at the surface compared to the experimental data. At temperature equals 533 K, the detrapped amount for 0.85 eV is not enough thus the peak at one micrometer has higher value than the experimental data. The large difference of the experimental data of the retention amount between 463 K and 533 K might again attribute to surface recombination effect. Fig. 7 shows the result of 200 eV deuterium incident on polycrystalline tungsten at 323 K with flux of 4×10^{19} $\mathrm{m^{-2}\ s^{-1}}$ and fluence of 3.2×10^{24} D $\mathrm{m^{-2}}$. Simulation results with and without the TGE term $\frac{DC_T\bar{V}_H}{RT}\frac{\partial^2 p}{\partial x^2}$ are compared to Alimov et al. [28] and Ning et al. [29].

3.2. Deuterium retention at 200 eV in SCW with various fluences

In this section, we modeled the single crystal tungsten (SCW) exposed to 200 eV deuterium ions with flux ($\approx 10^{19}$ $\mathrm{m^{-2}\ s^{-1}}$) to various fluences ($10^{21}/10^{25}$ D $\mathrm{m^{-2}}$) at 300 K. All results are compared with the experimental data from Skinner et al. [30], Alimov and Roth [28], Ogorodnikova et al. [20], Golubeva et al. [29,31] and Ning et al. [29]. The details of these experiments are slightly different and are listed in Table 3 with the tungsten types used, measurement methods, and temperature. The flux and fluence difference are listed in Table 4 for all experiments and simulations for comparison.

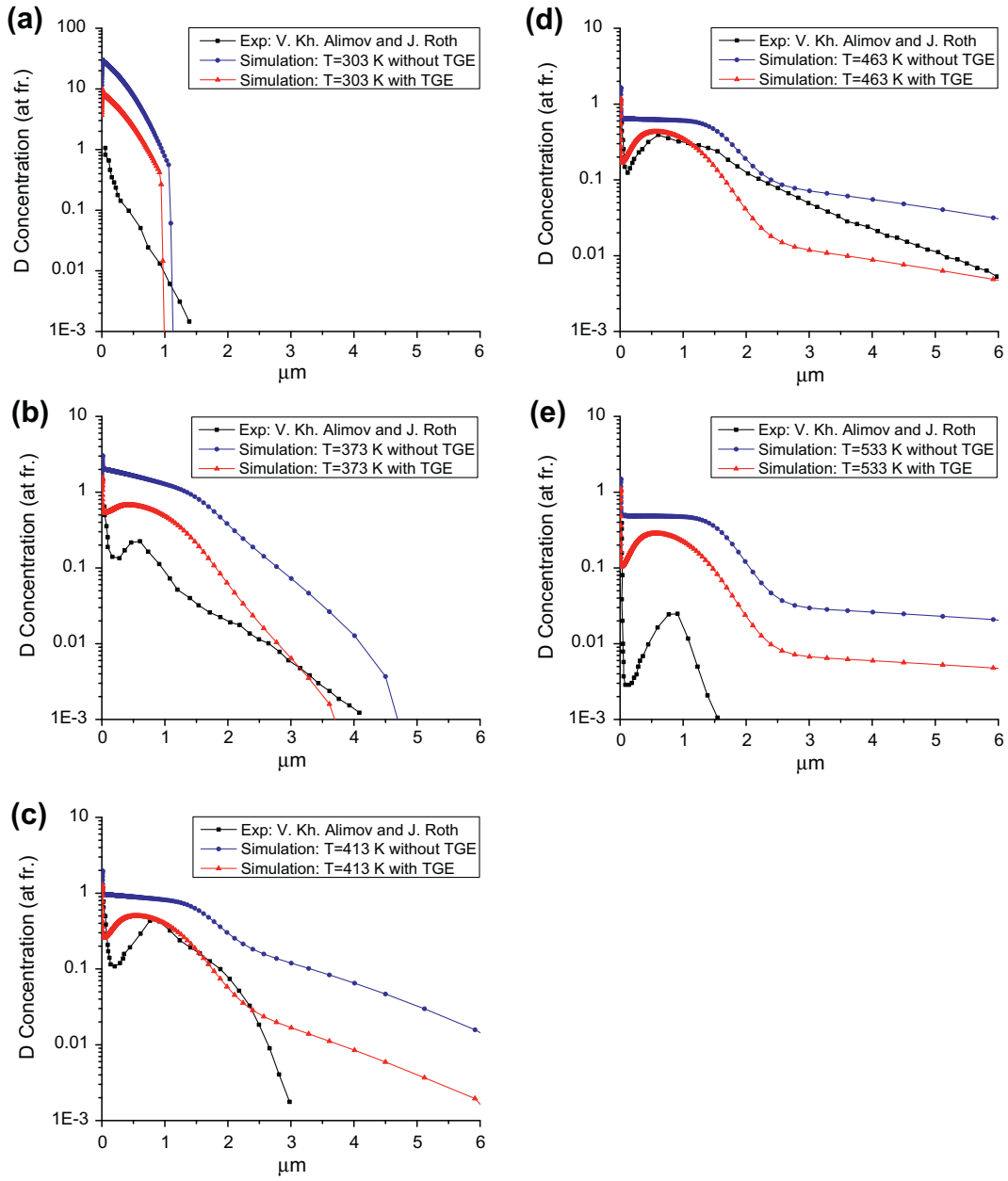

Fig. 6. Result for SCW exposed to 200 eV deuterium at various temperature (a) 303 K, (b) 373 K, (c) 413 K, (d) 463 K and (e) 533 K compared to Alimov and Roth [1].

In Fig. 8 we see that all the results are in a band region. Since the conditions are not exactly same for all presented work, it is hard to make a detailed conclusion. Alimov et al. use NRA to measure deuterium concentration and calculate the retentions amount from surface up to 7 μm, while TDS does not have a depth restriction. In the meantime, our model sums up all the deuterium in tungsten for up to 200 μm, so the amount is slightly larger than other results.

3.3. Deuterium retention at 200 eV in PCW at various temperatures

Simulation result is compared with experimental data using 200 eV deuterium incident on polycrystalline tungsten (PCW) from Alimov and Roth [1] and Ogorodnikova et al. [20], and also compared to modeling result by Ning et al. [17] The details between experiments and simulations are listed in Table 5. From Fig. 9 we can see that our result is in good agreement with other research. Alimov's result is lower compared to others because they again used NRA method and only count the retention from surface up to 7 μm, thus the difference becomes larger as temperature increases.

3.4. Deuterium retention of 500 eV in PCW at various temperatures

Fig. 10 shows the retention simulation result at various temperatures compared with the results of Roszell et al. [32] and Haasz et al. [33] Both experiments use polycrystalline tungsten and TDS measurement method. Table 6 lists the flux and fluence difference between experiments and simulation. For temperatures larger than 600 K, the estimated diffusion range $r = \sqrt{6Dt}$ would exceed the normal setting 200 μm, so we extended the simulation distance to 500 μm. At temperatures of 600–700 K we see drop in the experimental retention data. This might be the cause of temperature range that is transitioning from low detrapping energy

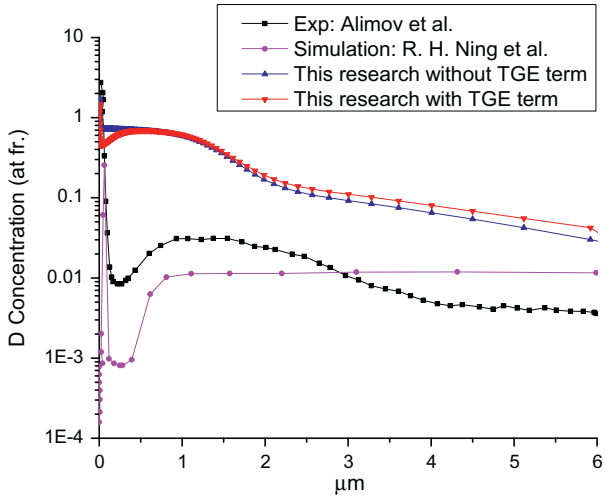

Fig. 7. Result of 200 eV deuterium incident on polycrystalline tungsten at 323 K. Comparison of our work with Alimov et al. [28] data and Ning et al. [29] simulations.

Table 3
Differences among various experiments.

	Skinner et al. [30] and Alimov et al. [28]	Ogorodnikova et al. [20]	Golubeva et al. [31]
W type	PCW	PCW	VPSW
Measure	NRA	TDS	TDS
Temperature	323 K	RT	RT

Table 4
Flux difference between researches.

	Flux
Skinner et al. [30] and Alimov et al. [28]	$(3.6 \pm 1.1) \times 10^{19}$ D m^{-2} s^{-1}
Ogorodnikova et al. [20]	$2.5–8 \times 10^{19}$ D m^{-2} s^{-1}
Golubeva et al. [31]	$\sim 5 \times 10^{19}$ D m^{-2} s^{-1}
Ning et al. [29]	4×10^{19} D m^{-2} s^{-1}
This research	5×10^{19} D m^{-2} s^{-1}

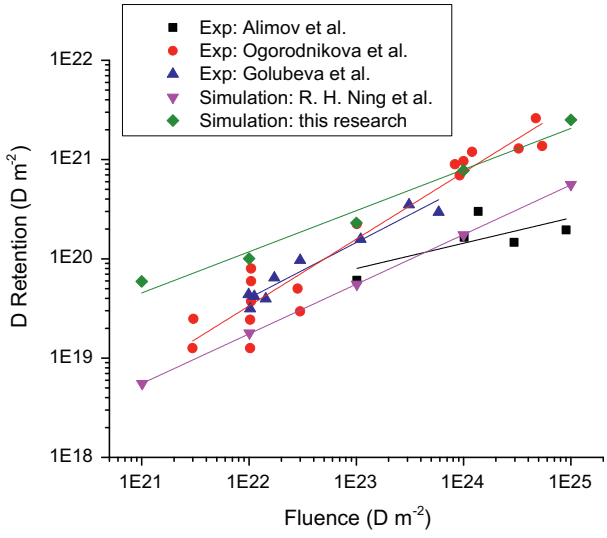

Fig. 8. Deuterium retention in tungsten with various fluences.

Table 5
Flux and fluence difference among various works.

	Flux	Fluence
Alimov et al. [1]	4×10^{19} D m^{-2} s^{-1}	1×10^{24} D m^{-2}
Ogorodnikova et al. [20]	$2.5–4 \times 10^{19}$ D m^{-2} s^{-1}	1×10^{24} D m^{-2}
Ning et al. [17]	4×10^{19} D m^{-2} s^{-1}	1×10^{24} D m^{-2}
This research	4×10^{19} D m^{-2} s^{-1}	1×10^{24} D m^{-2}

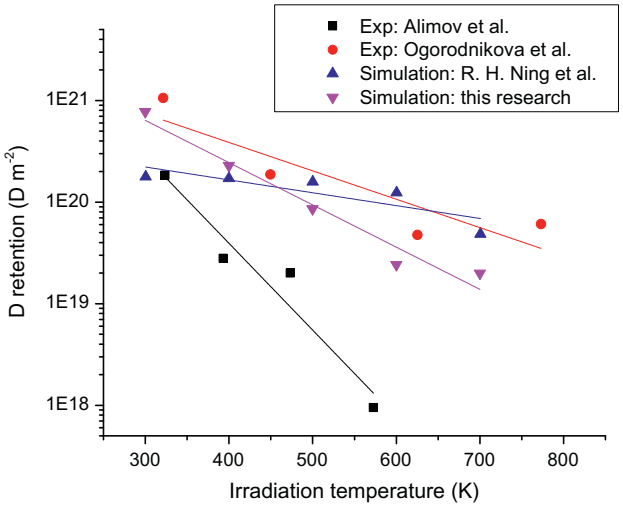

Fig. 9. Deuterium retention in polycrystalline tungsten at various temperatures.

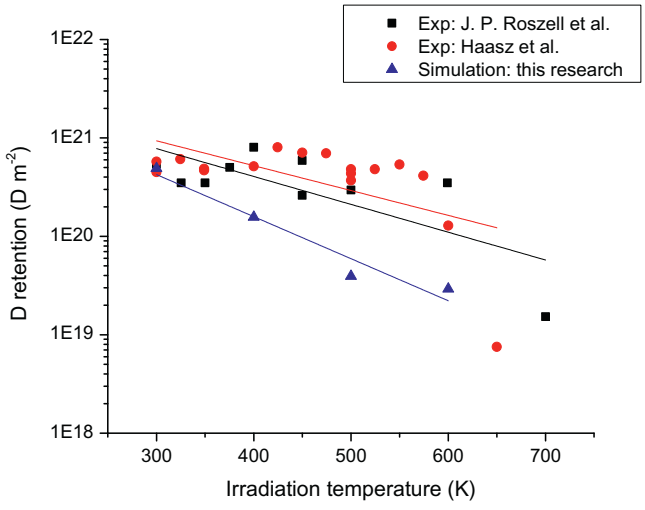

Fig. 10. Deuterium retention of 500 eV in polycrystalline tungsten at various temperatures.

Table 6
Flux and fluence difference between researches.

	Flux	Fluence
Roszell et al. [32]	3×10^{18} D m^{-2} s^{-1}	4×10^{23} D m^{-2}
Haasz et al. [33]	8×10^{19} D m^{-2} s^{-1}	1×10^{23} D m^{-2}
This research	3×10^{18} D m^{-2} s^{-1}	4×10^{23} D m^{-2}

dominated region to high detrapping energy dominated region. When the temperature is high our modeling predicts that the retention amount is smaller. This could be because of surface recombination coefficient is large at high temperature. For

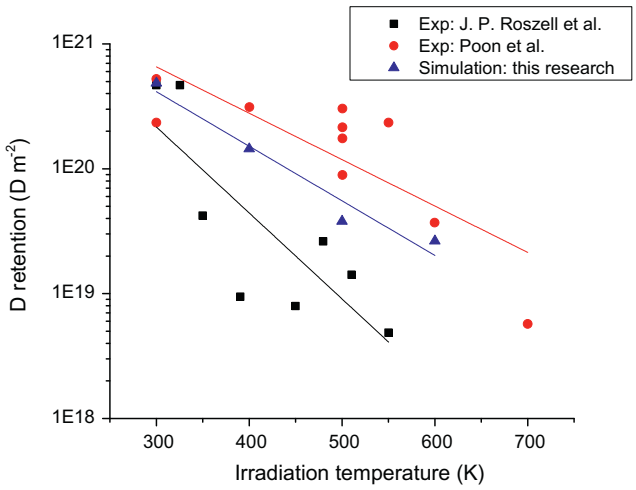

Fig. 11. Deuterium retention at 500 eV in single crystal tungsten at various temperatures.

Table 7
Flux and fluence difference between researches.

	Flux	Fluence
Roszell et al. [32]	3×10^{18} D m^{-2} s^{-1}	3×10^{23} D m^{-2}
Poon et al. [34]	$5 \sim 6 \times 10^{18}$ D m^{-2} s^{-1}	1×10^{24} D m^{-2}
This research	3×10^{18} D m^{-2} s^{-1}	3×10^{23} D m^{-2}

example, the surface recombination coefficient at 300 K is $K_r = 1.0423 \times 10^{-34}$ while at 600 K it is $K_r = 5.7753 \times 10^{-25}$ which is almost ten orders larger than the value at 300 K. The recombination flux at the surface and detail physics controlling this should be further understood and benchmarked.

3.5. Deuterium retention of 500 eV in SCW at various temperatures

Fig. 11 shows the retention simulation result at various temperature compared with Roszell et al. [32] and Poon et al. [33,34] both experiments use single crystal tungsten and TDS measurement method. The flux and fluence differences are listed in Table 7. The result value from Poon et al. [34] is larger than result from Roszell et al. [32] because their fluence is larger. Our result is in good agreement with the other two experiments.

4. Conclusions

We have developed models to study hydrogen isotope behavior in metallic plasma facing components in fusion reactors. The models integrate various effects that affect hydrogen isotope retention including implantation profile, diffusion, radiation and stress enhanced diffusion, trapping, detrapping, and surface recombination. From our simulation, we have benchmarked our models with other experimental and simulation results. The deuterium depth distributions qualitatively resembled the observed profile though they do not exactly fit the experiment profile very near the surface region. Furthermore, the total retention amounts are in good agreement with recent experimental and simulation data. Surface recombination is a very important factor controlling hydrogen isotope retention and permeation. More details need to be included in models to account for surface moving boundaries and impurity effects. For example, other mechanisms involving in irradiation and diffusion enhanced processes need to be considered in details. Also need to take into account surface build-up or erosion from plasma transient events, even when the implementation of moving boundaries due to sputtering erosion is considered in this model. Additional mechanisms such as surface segregation, impurities effect on surface recombination, chemical sputtering, mixing materials and neutron damage, are all play important roles in fusion energy realization and therefore need to be considered in future development of this simulation. A well-developed continuum model is necessary for predicting isotope species detail evolution to determine hydrogen isotope inventory and recycling. This continuum model that includes various important factors discussed in this work in an integrated and self-consistent description is very important in future reactor design and operation to predict hydrogen isotope behavior in plasma-facing components.

Acknowledgments

This work is partially supported by Department of Energy, Office of Fusion Energy Sciences and the National Science Foundation (PIRE) project.

References

[1] V.K. Alimov, J. Roth, Phys. Scr. T128 (2007) 6–13.
[2] A.N. Perevezentsev, A.C. Bell, L.A. Rivkis, V.M. Filin, V.V. Gushin, M.I. Belyakov, V.I. Bulkin, I.M. Kravchenko, I.A. Ionessian, Y. Torikai, M. Matsuyama, K. Watanabe, A.I. Markin, J. Nucl. Mater. 372 (2–3) (2008) 263–276.
[3] V.K. Alimov, J. Roth, S. Lindig, J. Nucl. Mater. 381 (3) (2008) 267–270.
[4] W.S. Gorsky, Physikalische Zeitschrift der Sowjetunion 8 (4) (1935) 457–471.
[5] J.V.G. Schaumann, G. Alefeld, Phys. Status Solidi 42 (1970).
[6] R. Cantelli, Mater. Sci. Eng., A 442 (1–2) (2006) 5–20.
[7] H.R. Sinning, Phys. Rev. Lett. 85 (15) (2000) 3201–3204.
[8] H.R. Sinning, R. Scarfone, G. Steckler, J. Alloy. Compd. 310 (2000) 219–223.
[9] M.I. Baskes, Sandia National Laboratories. Report, SAND83-8231, 1983.
[10] K.L. Wilson, R. Bastasz, R.A. Causey, D.K. Brice, B.L. Doyle, W.R. Wampler, W. Moller, B.M.U. Scherzer, T. Tanabe, Nucl. Fusion 1 (1991) 31–50.
[11] P. Sofronis, R.M. McMeeking, J. Mech. Phys. Solids 37 (3) (1989) 317–350.
[12] Abaqus Theory Manual.
[13] A.C. Hindmarsh, P.N. Brown, K.E. Grant, S.L. Lee, R. Serban, D.E. Shumaker, C.S. Woodward, Acm Trans. Math. Software 31 (3) (2005) 363–396.
[14] Sputtering by particle bombardment: experiments and computer calculations from threshold to MeV energies, Springer, 10.09. 2007, (2007).
[15] A.M. Hassanein, Fusion Technol. 8 (1) (1985) 1735–1741.
[16] O.V. Ogorodnikova, J. Roth, M. Mayer, J. Nucl. Mater. 313 (2003) 469–477.
[17] R.H. Ning, Y.G. Li, W.H. Zhou, Z. Zeng, X. Ju, J. Nucl. Mater. 430 (1–3) (2012) 20–26.
[18] C. Sang, X. Bonnin, M. Warrier, A. Rai, R. Schneider, J. Sun, D. Wang, Nucl. Fusion 52 (4) (2012).
[19] R. Frauenfelder, J. Vac. Sci. Technol. 6 (3) (1969) 388–397.
[20] O.V. Ogorodnikova, J. Roth, M. Mayer, J. Appl. Phys. 103 (3) (2008).
[21] P. Franzen, C. Garcia-Rosales, H. Plank, V.Kh. Alimov, J. Nucl. Mater. 1082 (1997) 241–243.
[22] C. GarciaRosales, P. Franzen, H. Plank, J. Roth, E. Gauthier, J. Nucl. Mater. 233 (1996) 803–808.
[23] T.M. Ahn, A Model for Hydrogen Induced Slow Crack Growth in Hydride Forming Metals, Department of Nuclear Energy, Brookhaven National Laboratory, BNL-NUREG-35596, 1984.
[24] T. Ohmi, A.T. Yokobori Jr., K. Takei, Diffus. Solids Liq. Vii 326–328 (2012) 626–631.
[25] R.A. Anderl, D.F. Holland, G.R. Longhurst, R.J. Pawelko, C.L. Trybus, C.H. Sellers, Fusion Technol. 21 (2) (1992) 745–752.
[26] P. Franzen, C. GarciaRosales, H. Plank, V.K. Alimov, J. Nucl. Mater. 241 (1997) 1082–1086.
[27] R.A. Causey, J. Nucl. Mater. 300 (2–3) (2002) 91–117.
[28] V.K. Alimov, J. Roth, M. Mayer, J. Nucl. Mater. 337 (1–3) (2005) 619–623.
[29] R.H. Ning, Y.G. Li, W.H. Zhou, Z. Zeng, X. Ju, Int. J. Mod. Phys. C 23 (6) (2012).
[30] C.H. Skinner, A.A. Haasz, V.K. Alimow, N. Bekris, R.A. Causey, R.E.H. Clark, J.P. Coad, J.W. Davis, R.P. Doerner, M. Mayer, A. Pisarev, J. Roth, T. Tanabe, Fusion Sci. Technol. 54 (4) (2008) 891–945.
[31] A.V. Golubeva, M. Mayer, J. Roth, V.A. Kurnaev, O.V. Ogorodnikova, J. Nucl. Mater. 363 (2007) 893–897.
[32] J.P. Roszell, J.W. Davis, A.A. Haasz, J. Nucl. Mater. 429 (1–3) (2012) 48–54.
[33] A.A. Haasz, J.W. Davis, M. Poon, R.G. Macaulay-Newcombe, J. Nucl. Mater. 258 (1998) 889–895.
[34] M. Poon, A.A. Haasz, J.W. Davis, R.G. Macaulay-Newcombe, J. Nucl. Mater. 313 (2003) 199–203.